ELSEVIER

Engineering Analysis with Boundary Elements 28 (2004) 1025–1034

ENGINEERING ANALYSIS with BOUNDARY ELEMENTS

www.elsevier.com/locate/enganabound

BEM solution for the Cauchy problem associated with Helmholtz-type equations by the Landweber method

L. Marin[a,*], L. Elliott[b], P.J. Heggs[c], D.B. Ingham[b], D. Lesnic[b], X. Wen[a]

[a]*School of the Environment, University of Leeds, Leeds LS2 9JT, UK*
[b]*Department of Applied Mathematics, University of Leeds, Leeds LS2 9JT, UK*
[c]*Department of Chemical Engineering, UMIST, P.O. Box 88, Manchester M60 1QD, UK*

Received 2 December 2003; revised 11 March 2004; accepted 17 March 2004

Available online 5 May 2004

Abstract

In this paper, an iterative algorithm based on the Landweber method in combination with the Boundary Element Method (BEM) is developed for solving the Cauchy problem for Helmholtz-type equations. A stopping regularizing criterion based on the residual of the BEM discretisation system of equations is also proposed.

Keywords: Boundary element method; Cauchy problem; Helmholtz-type equations; Inverse problem

1. Introduction

The Helmholtz equation arises naturally in many physical applications related to wave propagation and vibration phenomena. It is often used to describe the vibration of a structure [1], the acoustic cavity problem [2], the radiation wave [3] and the scattering of a wave [4]. Another important application of the Helmholtz equation is the problem of heat conduction in fins [5–7], and we focus on the later problem in this study. The well-posedness of the direct problems for the Helmholtz equation via the removal of the eigenvalues of the Laplacian operator is well established [8]. However, in many engineering problems, the boundary conditions are often incomplete, either in the form of underspecified and overspecified boundary conditions on different parts of the boundary or the solution is prescribed at some internal points in the domain. These are inverse problems and it is well known that they are generally ill-posed, i.e. the existence, uniqueness and stability of their solutions are not always guaranteed [9].

Unlike in direct problems, the uniqueness of the Cauchy problem is guaranteed without the necessity of removing the eigenvalues for the Laplacian. However, the Cauchy problem suffers from the non-existence and instability of the solution. A Boundary Element Method (BEM)-based acoustic holography technique using the singular value decomposition (SVD) for the reconstruction of sound fields generated by irregularly shaped sources has been developed by Bai [10]. The vibrational velocity, sound pressure and acoustic power on the vibrating boundary comprising an enclosed space have been reconstructed by Kim and Ih [11] who have used the SVD in order to obtain the inverse solution in the least-squares sense and to express the acoustic modal expansion between the measurement and source field. Wang and Wu [12] have developed a method employing the spherical wave expansion theory and a least-squares minimisation to reconstruct the acoustic pressure field from a vibrating object and their method has been extended to the reconstruction of acoustic pressure fields inside the cavity of a vibrating object by Wu and Yu [13]. DeLillo et al. [14] have detected the source of acoustical noise inside the cabin of a midsize aircraft from measurements of the acoustical pressure field inside the cabin by solving a linear Fredholm integral equation of the first kind. Recently, Marin et al. [15,16] have solved the Cauchy problem associated to the Helmholtz equation using the BEM in conjunction with an alternating iterative procedure consisting of obtaining successive solutions to well-posed mixed boundary value problems and with the conjugate gradient method (CGM), respectively.

* Corresponding author. Tel.: +44-113-343-6744; fax: + 44-113-343-6716.
E-mail address: liviu@env.leeds.ac.uk (L. Marin).

0955-7997/$ - see front matter © 2004 Elsevier Ltd. All rights reserved.
doi:10.1016/j.enganabound.2004.03.001

In this paper, we present and analyse the Landweber method [17] combined with the BEM, in order to solve the Cauchy problem for Helmholtz-type equations. This method reduces the problem to solving a sequence of two well-posed mixed boundary value problems. The problem is regularized by matching the number of iterations performed to the level of the noise in the input data and a stopping criterion is developed.

2. Mathematical formulation

Referring to heat transfer for the sake of the physical explanation, we assume that the temperature field $T(\underline{x})$ satisfies the Helmholtz equation in an open bounded domain $\Omega \subset \mathbb{R}^d$, where d is the dimension of the space in which the problem is posed, usually $d \in \{1,2,3\}$, namely

$$\mathscr{L}T(\underline{x}) \equiv (\Delta + k^2)T(\underline{x}) = \left(\sum_{j=1}^{d} \partial_j^2 + k^2\right) T(\underline{x}) = 0, \quad \underline{x} \in \Omega, \tag{1}$$

where $k = \alpha + \mathrm{i}\beta \in \mathbb{C}$, $\mathrm{i} = \sqrt{-1}$ and $k^2 \in \mathbb{R}$. For example, when $\alpha = 0$ and $\beta \in \mathbb{R}$, the partial differential equation (1) models the heat conduction in a fin [5–7], where T is the dimensionless local fin temperature, $\beta^2 = h/(\tilde{k}t)$, h is the surface heat transfer coefficient (W/(m^2 K)), $\tilde{k}$ is the thermal conductivity of the fin (W/(m K)) and t is the half-fin thickness (m). It should be mentioned that the Landweber method described in Section 3 is also valid in the case when k is real, i.e. $\alpha \in \mathbb{R}$ and $\beta = 0$. We now let $\nu(\underline{x})$ be the outward normal vector at the boundary $\Gamma \equiv \partial\Omega$ of class $\mathscr{C}^2$ and we define the flux at a boundary point $\underline{x} \in \Gamma$ by

$$\mathscr{N}T(\underline{x}) \equiv \Phi(\underline{x}) = (\partial T/\partial \nu)(\underline{x}), \qquad \underline{x} \in \Gamma. \tag{2}$$

The Cauchy problem under investigation requires solving the partial differential equation (1) subject to the boundary conditions

$$T(\underline{x}) = \tilde{T}(\underline{x}), \quad \mathscr{N}T(\underline{x}) = \tilde{\Phi}(\underline{x}), \qquad \underline{x} \in \Gamma_2, \tag{3}$$

where $\tilde{T}$ and $\tilde{\Phi}$ are prescribed functions and $\Gamma_2 \subset \Gamma$, meas$(\Gamma_2) > 0$. In the above formulation of the boundary conditions (3), it can be seen that the boundary Γ_2 is overspecified by prescribing both the temperature $T|_{\Gamma_2}$ and the flux $\Phi|_{\Gamma_2}$, whilst the boundary $\Gamma_1 = \Gamma \backslash \Gamma_2$ is underspecified since both the temperature $T|_{\Gamma_1}$ and the flux $\Phi|_{\Gamma_1}$ are unknown and have to be determined.

The Cauchy problem for Helmholtz-type equations is much more difficult to solve both analytically and numerically than the direct problem, since the solution does not satisfy the general conditions of well-posedness. In addition, it should be stressed that the Dirichlet, Neumann or mixed direct problems associated to Eq. (1) do not always have a unique solution due to the eigensolutions [8]. However, the Cauchy problem given by Eqs. (1) and (3) has a unique solution based on the analytical continuation property. Although this problem has a unique solution, it is well known that this solution is unstable with respect to small perturbations in the data on Γ_2, [9]. Thus the problem under investigation is ill-posed and we cannot use a direct approach, such as the Gauss elimination method, in order to solve the system of linear equations which arises from the discretisation of the partial differential equations (1) and the boundary conditions (3).

3. Landweber method

An iterative regularizing method for ill-posed problems is the Landweber iteration which was first investigated by Landweber [17] and Fridman [18]. It should be noted that this method is suitable to solve any linear inverse problem and for a general discussion on this method, we refer the reader to Ref. [19]. The main disadvantage of this method is the large numbers of iterations required to solve the problem in comparison with other iterative regularizing procedures, such as the CGM. The later method is known to be more powerful than the Landweber method [20–22]. However, the price that one pays is that the regularizing operator generated by the CGM is non-linear and hence the proof of the convergence for the CGM is more difficult and technical than that for the Lanweber method. Therefore, in this study, we have decided to apply the Landweber method for solving the Cauchy problem (1) and (3) associated with Helmholtz-type equations.

Assuming that $\Gamma \in \mathscr{C}^2$ is the union of two closed and disjoint parts Γ_1 and Γ_2, and $-k^2 \in \mathbb{R}$ is not an eigenvalue for the mixed problem for the Laplacian operator, we let T and v solve the problems

$$\begin{cases} \mathscr{L}T(\underline{x}) = 0, & \underline{x} \in \Omega, \\ T(\underline{x}) = \eta(\underline{x}), & \underline{x} \in \Gamma_1, \\ \mathscr{N}T(\underline{x}) = 0, & \underline{x} \in \Gamma_2, \end{cases} \tag{4}$$

and

$$\begin{cases} \mathscr{L}v(\underline{x}) = 0, & \underline{x} \in \Omega, \\ v(\underline{x}) = 0, & \underline{x} \in \Gamma_1, \\ \mathscr{N}v(\underline{x}) = \tilde{\Phi}(\underline{x}), & \underline{x} \in \Gamma_1, \end{cases} \tag{5}$$

respectively. Following the same lines of Johansson [23] where he considered the Oseen (generalised Stokes) system of linear hydrostatics, it can be shown that for $\eta \in L^2(\Gamma_1)$ and $\tilde{\Phi} \in L^2(\Gamma_2)$, both problems (4) and (5) have unique solutions $T \in L^2(\Omega)$ and $v \in L^2(\Omega)$, respectively, and the operators

$$\mathscr{K} : L^2(\Gamma_1) \to L^2(\Gamma_2), \qquad \eta \to \mathscr{K}\eta = T|_{\Gamma_2}, \tag{6}$$

$$\mathscr{K}_1 : L^2(\Gamma_2) \rightarrow L^2(\Gamma_2), \qquad \tilde{\Phi} \rightarrow \mathscr{K}_1 \tilde{\Phi} = v|_{\Gamma_2}, \tag{7}$$

are well-defined. Moreover, the operator $\mathscr{K}$ is linear, compact and injective, and its adjoint is given by

$$\mathscr{K}^* : L^2(\Gamma_2) \rightarrow L^2(\Gamma_1), \qquad \xi \rightarrow \mathscr{K}^* \xi = -\mathscr{N}^* v|_{\Gamma_1}, \tag{8}$$

where $v \in L^2(\Omega)$ is the solution to the following adjoint problem:

$$\begin{cases} \mathscr{L}^* v(\underline{x}) = 0, & \underline{x} \in \Omega, \\ v(\underline{x}) = 0, & \underline{x} \in \Gamma_1, \\ \mathscr{N}^* v(\underline{x}) = \xi(\underline{x}), & \underline{x} \in \Gamma_2, \end{cases} \tag{9}$$

Here $\mathscr{L}^*$ and $\mathscr{N}^*$ are the adjoint operators to $\mathscr{L}$ and $\mathscr{N}$ defined by Eqs. (1) and (3), respectively, and in the case of Helmholtz-type equations, they are given by $\mathscr{L}^* = \mathscr{L}$ and $\mathscr{N}^* = \mathscr{N}$. It should be noted that finding a solution to the Cauchy problems (1) and (3) is then equivalent to finding $\eta \in L^2(\Gamma_1)$ such that

$$\mathscr{K} \eta = \tilde{T} - \mathscr{K}_1 \tilde{\Phi}. \tag{10}$$

If such a solution η exists then by definitions (6) and (7) we have

$$T|_{\Gamma_2} = \tilde{T} - v|_{\Gamma_2}, \tag{11}$$

where T and v are the unique solutions in $L^2(\Omega)$ of the problems (4) and (5), respectively. Hence, $T + v$ is a solution to the Cauchy problems (1) and (3). Since $\mathscr{K}$ is a compact operator, it follows that $\mathscr{K}$ has no bounded inverse and, therefore, Eq. (10) is an ill-posed operator equation which requires the use of regularization methods.

In order to solve the Cauchy problems (1) and (3), the following iterative algorithm is proposed:

Step 1
Set $n = 0$. Choose an approximation $\eta^{(0)} \in L^2(\Gamma_1)$ for $T|_{\Gamma_1}$.
Step 2
Solve the well-posed mixed boundary value problem

$$\begin{cases} \mathscr{L} T^{(n)}(\underline{x}) = 0, & \underline{x} \in \Omega, \\ T^{(n)}(\underline{x}) = \eta^{(n)}(\underline{x}), & \underline{x} \in \Gamma_1, \\ \mathscr{N} T^{(n)}(\underline{x}) \equiv (\partial T^{(n)}/\partial \nu)(\underline{x}) = \tilde{\Phi}(\underline{x}), & \underline{x} \in \Gamma_2, \end{cases} \tag{12}$$

in order to determine $\mathscr{N} T^{(n)}(\underline{x}) \equiv (\partial T^{(n)}/\partial \nu)(\underline{x})$ for $\underline{x} \in \Gamma_1$ and $T^{(n)}(\underline{x})$ for $\underline{x} \in \Gamma_2$.
Step 3
Having constructed the approximation $T^{(n)}(\underline{x})$ for $\underline{x} \in \Gamma_2$, the adjoint problem

$$\begin{cases} \mathscr{L}^* v^{(n)}(\underline{x}) = 0, & \underline{x} \in \Omega, \\ v^{(n)}(\underline{x}) = 0, & \underline{x} \in \Gamma_1, \\ \mathscr{N}^* v^{(n)}(\underline{x}) \equiv (\partial v^{(n)}/\partial \nu)(\underline{x}) = T^{(n)}(\underline{x}) - \tilde{T}(\underline{x}), & \underline{x} \in \Gamma_1, \end{cases} \tag{13}$$

is solved to determine $\eta^{(n+1)}(\underline{x}) = \eta^{(n)}(\underline{x}) + \gamma \mathscr{N}^* v^{(n)}(\underline{x})$ for $\underline{x} \in \Gamma_1$, where $\gamma > 0$ is a constant to be prescribed.
Step 4
Set $n = n + 1$ and repeat steps 2 and 3 until a prescribed stopping criterion is satisfied.

We are now able to prove the following convergence result:

Theorem 1. *Let $T \in L^2(\Omega)$ be the solution to the Cauchy problems* (1) and (3), *and assume that γ satisfies $0 < \gamma < 1/\|\mathscr{K}\|^2$. Let $T^{(n)}$ be the n*th *approximate solution to the algorithm described above. Then*

$$\lim_{n \rightarrow \infty} \|T^{(n)} - T\|_{L^2(\Omega)} = 0, \tag{14}$$

for any initial data $\eta^{(0)} \in L^2(\Gamma_1)$.

Proof. The operator equation to be solved is Eq. (10). The function $\eta = T|_{\Gamma_1}$ is a solution of the operator equation (10) and it is unique since $\mathscr{K}$ is injective. From the above algorithm and expressions (8), (10) and (11), it follows that

$$\begin{aligned} \eta^{(n)} &= \eta^{(n-1)} + \gamma \mathscr{N}^* v^{(n-1)}|_{\Gamma_2} \\ &= \eta^{(n-1)} - \gamma \mathscr{K}^* (T^{(n-1)}|_{\Gamma_2} - \tilde{T}) \\ &= \eta^{(n-1)} - \gamma \mathscr{K}^* [\mathscr{K} \eta^{(n-1)} - (T - \mathscr{K}_1 \tilde{\Phi})]. \end{aligned} \tag{15}$$

This is the Landweber iteration procedure for solving the operator equation (10) and the sequence $\{\eta^{(n)}\}_{n \geq 0}$ converges to η in $L^2(\Gamma_1)$ since $0 < \gamma < 1/\|\mathscr{K}\|^2$, [19]. Applying Lemma 6.3 from Ref. [23], it follows that the sequence $\{T^{(n)}\}_{n \geq 0}$ converges to T in $L^2(\Omega)$. □

4. Boundary element method

The Helmholtz-type equation (1) can also be formulated in integral form [8] as

$$c(\underline{x}) T(\underline{x}) + \int_{\Gamma} \frac{\partial E(\underline{x}, \underline{y})}{\partial \nu(\underline{y})} T(\underline{y}) \mathrm{d}\Gamma(\underline{y}) = \int_{\Gamma} E(\underline{x}, \underline{y}) \Phi(\underline{y}) \mathrm{d}\Gamma(\underline{y}) \tag{16}$$

for $\underline{x} \in \overline{\Omega} = \Omega \cup \Gamma$, where the first integral is taken in the sense of the Cauchy principal value, $c(\underline{x}) = 1$ for $\underline{x} \in \Omega$ and $c(\underline{x}) = 1/2$ for $\underline{x} \in \Gamma$ (smooth), and E is the fundamental solution for the Helmholtz-type equation (1), which in two-dimensions is given by

$$E(\underline{x}, \underline{y}) = \frac{\mathrm{i}}{4} H_0^{(1)}(k|\underline{x} - \underline{y}|), \tag{17}$$

with $H_0^{(1)}$ the Hankel function of order zero of the first kind. Using standard arguments for linear elliptic partial differential equations, it can be shown that the integral equation representation (16) with Cauchy or mixed data is equivalent to the original equation (1) with Cauchy data (3) or mixed data (12) or (13) on the closed and disjoint boundary parts

Γ_1 and Γ_2, in the sense that the traces of the weak solution satisfy the integral equation and, conversely, the solution of the integral equation inserted into Green's formula (16) yields the solution of the Cauchy or mixed boundary value problems, see Ref. [24] for two-dimensions and Ref. [25] for three-dimensions. It should be noted that in practice the boundary integral equation (16) can rarely be solved analytically and thus a numerical approximation is required.

A BEM with constant boundary elements [15,16] is used in order to discretise the problem given by Eqs. (1) and (3). If the boundaries Γ_1 and Γ_2 are discretised into N_1 and N_2 constant boundary elements, respectively, such that $N = N_1 + N_2$, then on applying Eq. (16) at each node on Γ, we arrive at the following system of linear algebraic equations

$$\mathbf{A}\underline{T} = \mathbf{B}\underline{\Phi}. \tag{18}$$

Here **A** and **B** are matrices which depend solely on the geometry of the boundary Γ and the vectors $\underline{T}$ and $\underline{\Phi}$ consist of the discretised values of the temperature and the flux, respectively, on the boundary Γ. The system of equations (16), together with appropriate boundary conditions, is solved for each of the the direct well-posed mixed boundary value problems (12) and (13) at each iteration, n, of the algorithm presented in Section 3.

5. Numerical results and discussion

In this section, we illustrate the numerical results obtained using the iterative Landweber algorithm proposed in Section 3 combined with the BEM described in Section 4 for solving the two mixed well-posed problems (12) and (13) at each iteration. In addition, we investigate the convergence with respect to the mesh size discretisation and the number of iterations when the data is exact and the stability when the data is perturbed by noise.

5.1. Examples

In order to present the performance of the numerical method proposed, we solve the Cauchy problems (1) and (3) in a smooth two-dimensional geometry ($d = 2$), namely the annulus $\Omega = \{\underline{x} = (x_1, x_2) | R_i^2 < x_1^2 + x_2^2 < R_0^2\}$, $R_i = 0.5$ and $R_0 = 1.0$. We assume that the boundary Γ of the domain Ω is divided into two disjointed parts, namely $\Gamma_1 = \{\underline{x} \in \Gamma | x_1^2 + x_2^2 = R_i^2\}$ and $\Gamma_2 = \{\underline{x} \in \Gamma | x_1^2 + x_2^2 = R_0^2\}$, and the outer boundary Γ_2 is overspecified by the prescription of both the temperature and the flux while the inner boundary Γ_1 is unspecified with both the temperature and the flux unknown. We consider the following analytical solutions for the temperature in the domain Ω, which have also been used in Refs. [15,16]:

Example 1. ($\mathscr{L} \equiv \Delta - \beta^2$, $\beta \in \mathbb{R}$)

$$T^{(\mathrm{an})}(\underline{x}) = \exp(a_1 x_1 + a_2 x_2), \qquad \underline{x} = (x_1, x_2) \in \Omega, \tag{19}$$

where $k = \alpha + \mathrm{i}\beta$, $\alpha = 0$, $\beta = 2.0$, $a_1 = 1.0$ and $a_2 = \sqrt{\beta^2 - a_1^2}$, which corresponds to a heat flux on the boundary Γ given by

$$(\partial T^{(\mathrm{an})}/\partial \nu)(\underline{x}) = (a_1 \nu_1(\underline{x}) + a_2 \nu_2(\underline{x}))\exp(a_1 x_1 + a_2 x_2), \quad \underline{x} = (x_1, x_2) \in \Gamma. \tag{20}$$

Example 2. ($\mathscr{L} \equiv \Delta + \alpha^2$, $\alpha \in \mathbb{R}$)

$$T^{(\mathrm{an})}(\underline{x}) = \cos(a_1 x_1 + a_2 x_2), \qquad \underline{x} = (x_1, x_2) \in \Omega, \tag{21}$$

where $k = \alpha + \mathrm{i}\beta$, $\alpha = 2.0$, $\beta = 0$, $a_1 = 1.0$ and $a_2 = \sqrt{\alpha^2 - a_1^2}$, which corresponds to a heat flux on the boundary Γ given by

$$(\partial T^{(\mathrm{an})}/\partial \nu)(\underline{x}) = -(a_1 \nu_1(\underline{x}) + a_2 \nu_2(\underline{x}))\sin(a_1 x_1 + a_2 x_2), \quad \underline{x} = (x_1, x_2) \in \Gamma. \tag{22}$$

For the BEM discretisation of the problems (12) and (13), we have used various numbers of constant boundary elements, namely $N \in \{40, 80, 160\}$ and $N_1 = N_2 = N/2$.

5.2. Convergence of the algorithm

An arbitrary function $\eta^{(0)} \in L^2(\Gamma_1)$ may be specified as an initial guess for the temperature on Γ_1. For the examples considered, this initial guess has been chosen as

$$\eta^{(0)}(\underline{x}) = T^{(0)}(\underline{x}) = 0, \qquad \underline{x} \in \Gamma_1, \tag{23}$$

and this choice ensures that the initial guess is not too close to the exact values $T^{(\mathrm{an})}$.

In order to investigate the convergence of the algorithm, at every iteration we evaluate the accuracy errors defined by

$$e_T = \|T^{(n)} - T^{(\mathrm{an})}\|_{L^2(\Gamma_1)}, \quad e_\Phi = \|\Phi^{(n)} - \Phi^{(\mathrm{an})}\|_{L^2(\Gamma_1)}, \tag{24}$$

where $T^{(n)}$ and $\Phi^{(n)}$ are the temperature and the flux on the boundary Γ_1 retrieved after n iterations, respectively, and each iteration consists of solving the two mixed well-posed problems (12) and (13) using the BEM. The error in predicting the temperature inside the solution domain Ω may also be evaluated by using the expression

$$e_\Omega = \|T^{(n)} - T^{(\mathrm{an})}\|_{L^2(\Omega)}. \tag{25}$$

However, this is not pursued here since e_Ω has an evolution similar to that of the errors e_T and e_Φ, as at each iteration the values of the temperature inside the solution domain are retrieved from the values of the temperature T and the flux Φ on the boundary Γ.

Fig. 1(a) and (b) shows the accuracy errors e_T and e_Φ, respectively, as functions of the number of iterations, n, obtained for the Cauchy problem given by Example 1 for $N \in \{40, 80, 160\}$ when using 'exact boundary data' for the inverse problem, i.e. boundary data obtained by solving

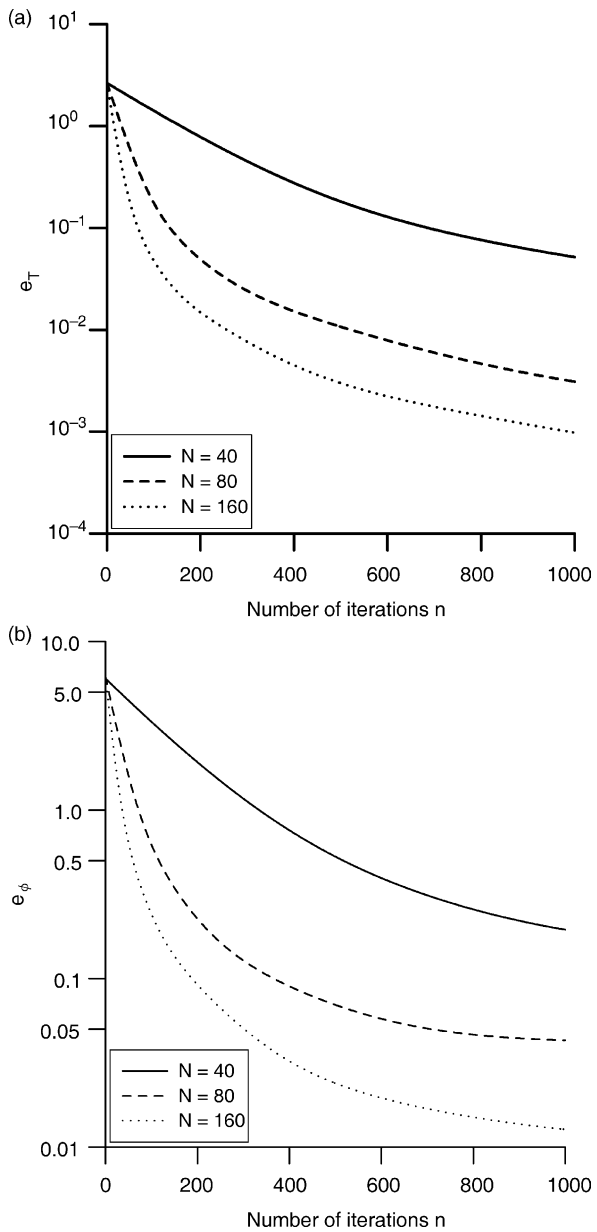

Fig. 1. The accuracy errors (a) $e_T = \|T^{(n)} - T^{(\mathrm{an})}\|_{L^2(\Gamma_1)}$, and (b) $e_\Phi = \|\Phi^{(n)} - \Phi^{(\mathrm{an})}\|_{L^2(\Gamma_1)}$ as functions of the number of iterations, n, obtained with exact input data $\tilde{T}|_{\Gamma_2}$ and $N = 40$ (—), $N = 80$ (– – –) and $N = 160$ (···) boundary elements, for Example 1.

the direct well-posed problem given by Eq. (1) subject to the boundary conditions

$$\Phi(\underline{x}) \equiv (\partial T/\partial \nu)(\underline{x}) = \Phi^{(\mathrm{an})}(\underline{x}), \quad \underline{x} \in \Gamma_1,$$
$$T(\underline{x}) = T^{(\mathrm{an})}(\underline{x}), \quad \underline{x} \in \Gamma_2. \tag{26}$$

It can be seen from these figures that both errors e_T and e_Φ keep decreasing, even after a large number of iterations, e.g. $N = 1000$, and, as expected, $e_T < e_\Phi$, i.e. temperatures are more accurate than fluxes. Furthermore, as N increases, the errors e_T and e_Φ decrease showing that $N \geq 80$ ensures a sufficiently fine discretisation for the accuracy to be achieved. Although not presented here, it is reported that the same conclusions have been obtained for the Cauchy problem given by Example 2. From Fig. 1(a) and (b), it can be concluded that the iterative algorithm described in Section 3 is convergent with respect to increasing the number of iterations, provided that exact boundary data is prescribed.

The numerical solutions for the temperature $T|_{\Gamma_1}$ obtained after $n = 1000$ iterations for Examples 1 and 2 are presented in Fig. 2(a) and (b), respectively. From these figures, it can be seen that the accuracy in predicting the temperature on the boundary Γ_1 is very good for both examples considered. The behaviour of the numerical solution for the flux $\Phi|_{\Gamma_1}$, along

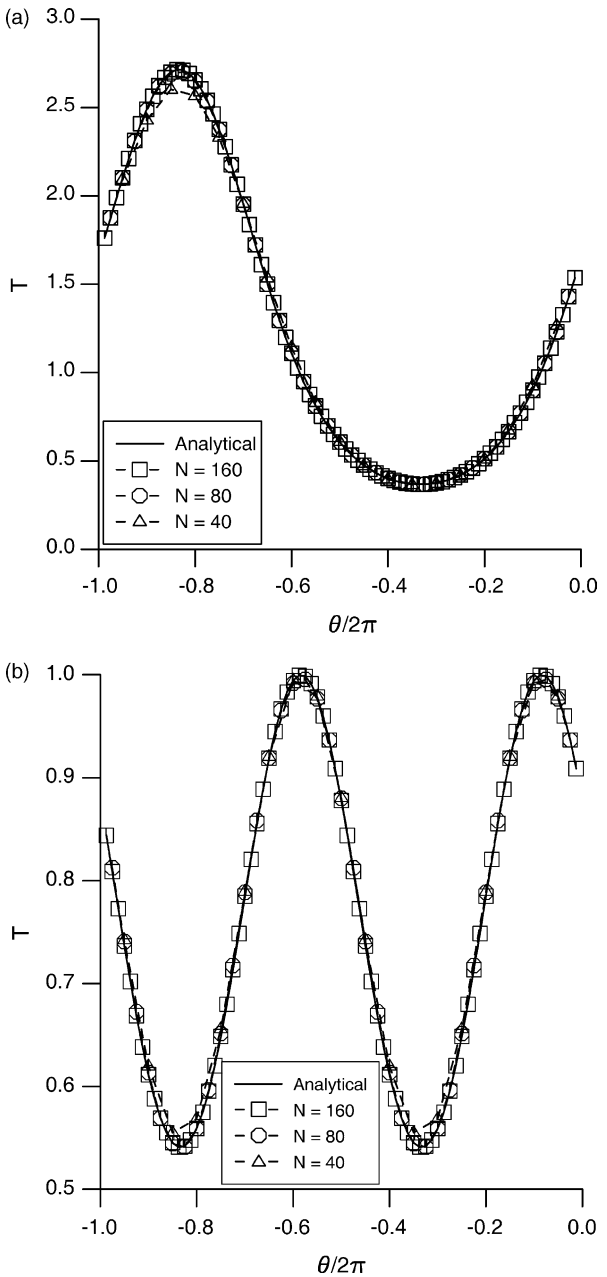

Fig. 2. The analytical solution $T^{(\mathrm{an})}$ (—) and the numerical solution $T^{(\mathrm{num})}$ obtained with exact input data $\tilde{T}|_{\Gamma_2}$ and $N = 40$(–△–), $N = 80$ (–○–) and $N = 160$ (–□–) boundary elements, for (a) Example 1, and (b) Example 2.

with the analytical flux solution on the boundary Γ_1, after $n = 1000$ iterations for Examples 1 and 2 is presented in Fig. 3(a) and (b), respectively. As expected, the errors in predicting the flux $\Phi|_{\Gamma_1}$ are larger than the errors in predicting the temperature $T|_{\Gamma_1}$ since the flux contains higher-order derivatives. Moreover, from Figs. 2 and 3, it can be seen that the numerical solutions for the temperature $T|_{\Gamma_1}$ and the flux $\Phi|_{\Gamma_1}$ are very accurate for both Examples 1 and 2, provided that $N \geq 80$.

In Fig. 4(a) and (b), we present the numerical solution for the temperature T obtained after $n = 1000$ iterations and using various numbers $N \in \{40, 80, 160\}$ of boundary elements in comparison with its analytical value at the internal points $\underline{x}$ located on an interior circle, $\Gamma_r = \{\underline{x} = (x_1, x_2) = 0.75\}$, and along a radius, $\Gamma_\theta = \{\underline{x} = (x_1, x_2) | \theta(\underline{x}) = \pi/3\}$, respectively, for Example 1. From these figures it can be seen that the numerical temperature retrieved at the internal points considered represents of a very good approximation of its exact value and it converges to the analytical solution within $N = 80$ boundary elements. Similar results have been obtained for

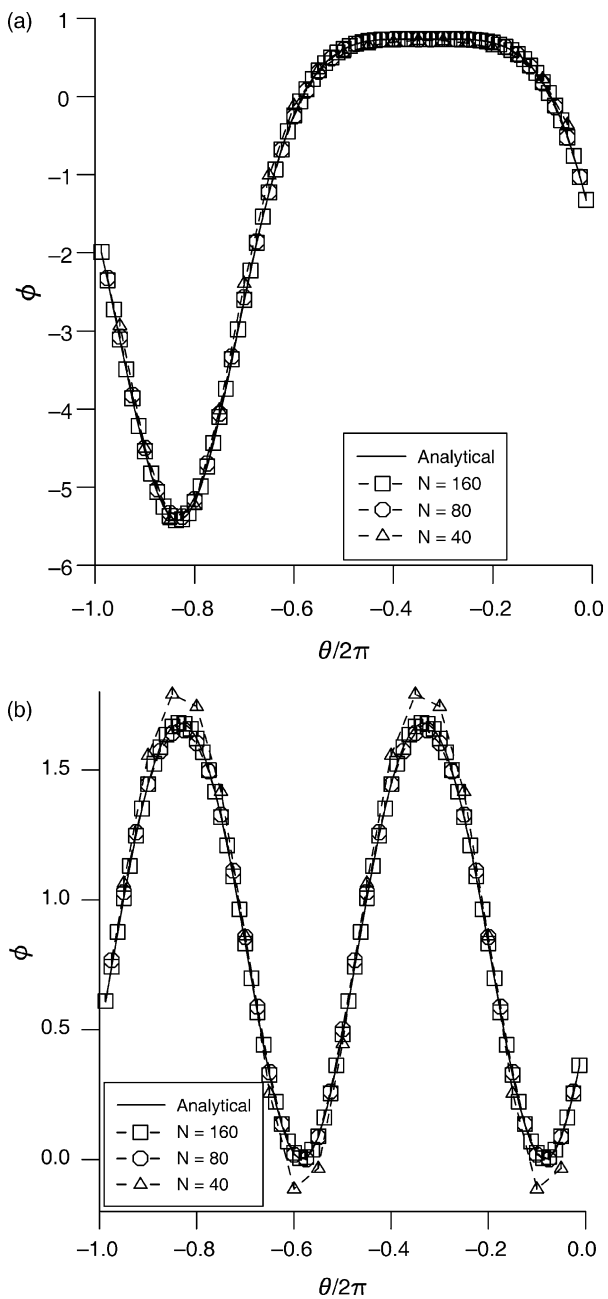

Fig. 3. The analytical solution $\Phi^{(an)}$ (—) and the numerical solution $\Phi^{(num)}$ obtained with exact input data $\tilde{T}|_{\Gamma_2}$ and $N = 40$ (–△–), $N = 80$ (–○–) and $N = 160$ (–□–) boundary elements, for (a) Example 1, and (b) Example 2.

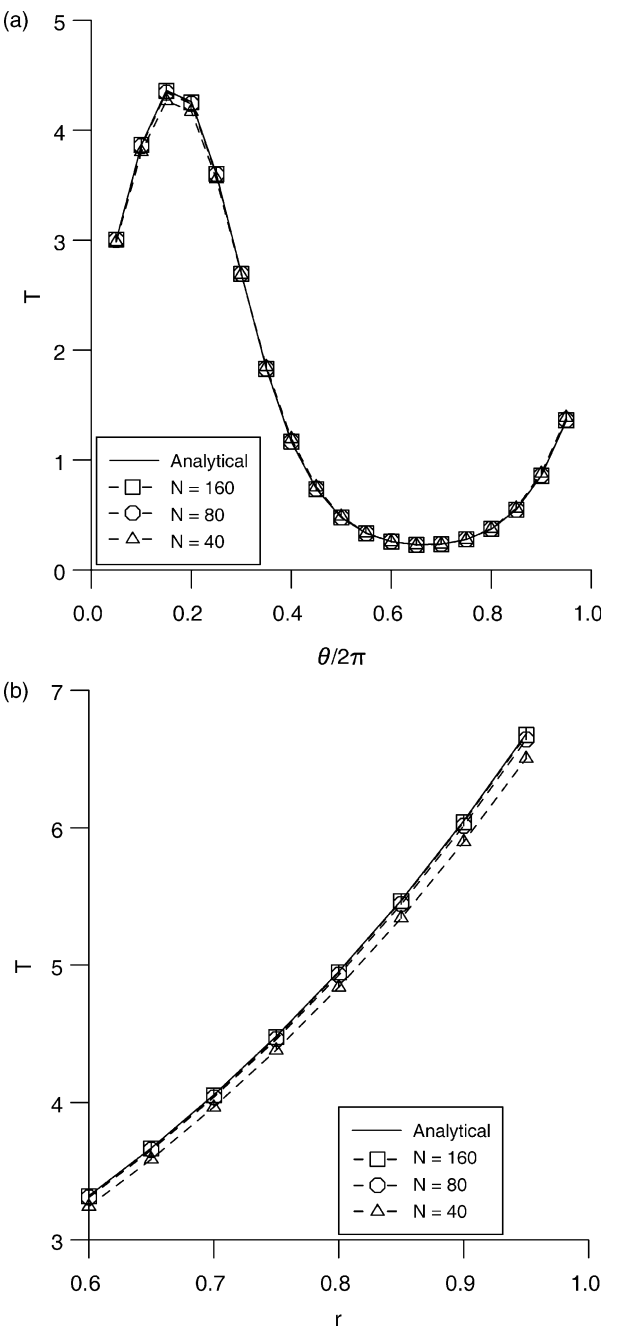

Fig. 4. The analytical solution $T^{(an)}$ (—) and the numerical solution $T^{(num)}$ obtained with exact input data $\tilde{T}|_{\Gamma_2}$ and $N = 40$ (–△–), $N = 80$ (–○–) and $N = 160$ (–□–) boundary elements, at the internal points (a) $\underline{x} \in \Gamma_r$, and (b) $\underline{x} \in \Gamma_\theta$, for Example 1.

the Cauchy problem corresponding to Example 2 and hence they are not presented here.

For the Cauchy problem investigated in this paper, it was found that the proposed iterative BEM algorithm produces an accurate and convergent numerical solution for both the missing boundary temperature and flux, as well as the temperature inside the solution domain, with respect to increasing the number of iterations, n, and the number of boundary elements, N, provided that exact input data is used.

5.3. Stopping criterion

Once the convergence with respect to increasing N of the numerical solution to the exact solution has been established, we fix $N = 80$ and investigate the stability of the numerical solution for Example 2 only. Fig. 5 presents the accuracy errors e_T and e_Φ for various levels of Gaussian random noise $p \in \{1, 2, 3\}\%$ added into the temperature data $\tilde{T}|_{\Gamma_2}$. From this figure, it can be seen that as p decreases then e_T and e_Φ decrease. However, the errors in predicting the temperature and the flux on the underspecified boundary Γ_1 decrease up to a certain iteration number and after that they start increasing. If the iterative process is continued beyond this point then the numerical solutions lose their smoothness and become highly oscillatory and unbounded, i.e. unstable. Therefore, a regularizing stopping criterion must be used in order to terminate the iterative process at the point where the errors in the numerical solutions start increasing.

In a direct approach, the discretisation of the boundary conditions (3) provides the values of $2N_2$ of the unknowns and the problem reduces to solving a system of N equations with $2N_1$ unknowns which can generically be written as

$$\mathbf{C}\underline{X} = \underline{F}, \tag{27}$$

where $\underline{F}$ is computed using the boundary conditions (3), the matrix $\mathbf{C}$ depends solely on the geometry of the boundary Γ and the vector $\underline{X}$ contains the unknown values of the temperature and the flux on the boundary Γ_1.

If we evaluate the Euclidean norm of the vector $\mathbf{C}\underline{X} - \underline{F}$ then this should tend to zero as $\underline{X}$ tends to the exact solution. Hence after each iteration, we evaluate the error

$$E = \|\mathbf{C}\underline{X}^{(n)} - \underline{F}\|_2, \tag{28}$$

where $\underline{X}^{(n)}$ is the vector obtained from the values of the temperature and the flux on the boundary Γ_1 retrieved after n iterations. The error E includes information on both the temperature and the flux and it is expected to provide an appropriate stopping criterion. Indeed, if we investigate the error E obtained at every iteration for various levels of Gaussian random noise added into the input temperature data $\tilde{T}|_{\Gamma_2}$, we obtain the curves graphically represented in Fig. 6. It can be seen from this figure, for all levels of noise considered, that the error E decreases up to a certain iteration number after which it reaches a plateau, and this

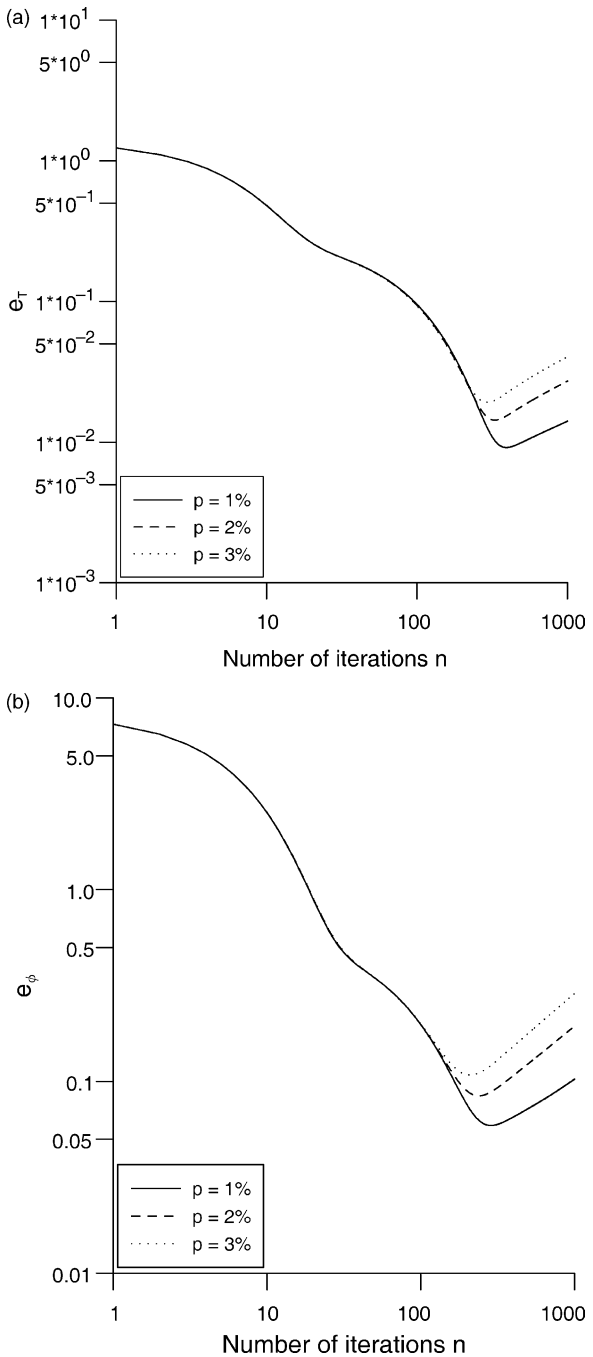

Fig. 5. The accuracy errors (a) $e_T = \|T^{(n)} - T^{(\mathrm{an})}\|_{L^2(\Gamma_1)}$, and (b) $e_\Phi = \|\Phi^{(n)} - \Phi^{(\mathrm{an})}\|_{L^2(\Gamma_1)}$ as functions of the number of iterations, n, obtained with $N = 80$ boundary elements and various levels of noise $p = 1\%$ (—), $p = 2\%$ (– – –) and $p = 3\%$ (···) added into the input data $\tilde{T}|_{\Gamma_2}$, for Example 2.

indicates the necessity to terminate the iterative process. By comparing Figs. 5(a), (b) and 6, it can be seen, for various levels of noise, that the corner corresponding to the beginning of the plateau region in the error E occurs at about the same point where the the minimum in the accuracy errors e_T and e_Φ appears. Therefore, the optimum point where the iterations should be ceased may be identified by locating the corner corresponding to the plateau region in

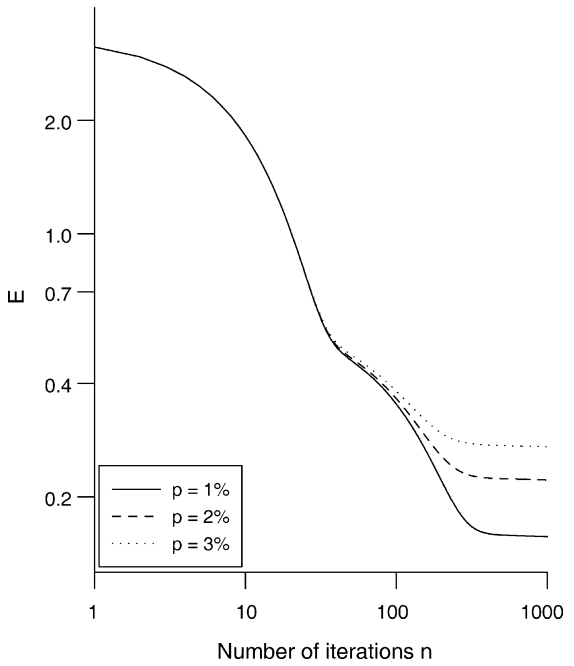

Fig. 6. The convergence error $E = \|\mathbf{C}\underline{X}^{(n)} - \underline{F}\|_2$ as a function of the number of iterations, n, obtained with $N = 80$ boundary elements and various levels of noise $p = 1\%$ (—), $p = 2\%$ (– – –) and $p = 3\%$ (–△–) added into the input data $\tilde{T}|_{\Gamma_2}$, for Example 2.

the error E. Although not illustrated here, it is reported that similar results have been obtained for Example 1. As mentioned in Section 5.2, for exact data, the iterative process is convergent with respect to increasing the number of iterations, n, since the accuracy errors e_T and e_Φ keep decreasing even after a large number of iterations, see Fig. 1(a) and (b). It should be noted in this case that a stopping criterion is not necessary since the numerical solution is convergent with respect to increasing the number of iterations. However, even in this case, the errors E, e_T and e_Φ have a similar behaviour and the error E may be used to stop the iterative process at the point where the rate of convergence is very small and no substantial improvement in the numerical solution is obtained even if the iterative process is continued. Therefore, it can be concluded that the regularizing stopping criterion proposed is very efficient in locating the point where the errors start increasing and the iterative process should be ceased.

5.4. Stability of the algorithm

Based on the stopping criterion described in Section 5.3, the numerical results obtained for the temperature T and the flux Φ on the boundary Γ_1 for Example 2 are presented in Fig. 7(a) and (b), respectively, for various levels of noise added into the temperature data on the boundary Γ_2. In Fig. 8(a) and (b), we present the numerical solution for the temperature T for Example 2 obtained using the stopping criterion described in Section 5.3 and various levels of noise added into the temperature data on the boundary Γ_2 in comparison with its analytical value at the internal points $\underline{x}$ located on an interior circle, $\Gamma_r = \{\underline{x} = (x_1, x_2) | r(\underline{x}) = 0.75\}$, and along a radius, $\Gamma_\theta = \{\underline{x} = (x_1, x_2) | \theta(\underline{x}) = \pi/3\}$, respectively. From Figs. 7 and 8, it can be seen that the numerical solution is a stable approximation to the exact solution, free of unbounded and rapid oscillations, and it converges to the exact solution as the level of noise, p, added into the input boundary data decreases. Similar results have been obtained for the Cauchy problem corresponding to Example 1 and hence they are not presented here. The same conclusion can be drawn from

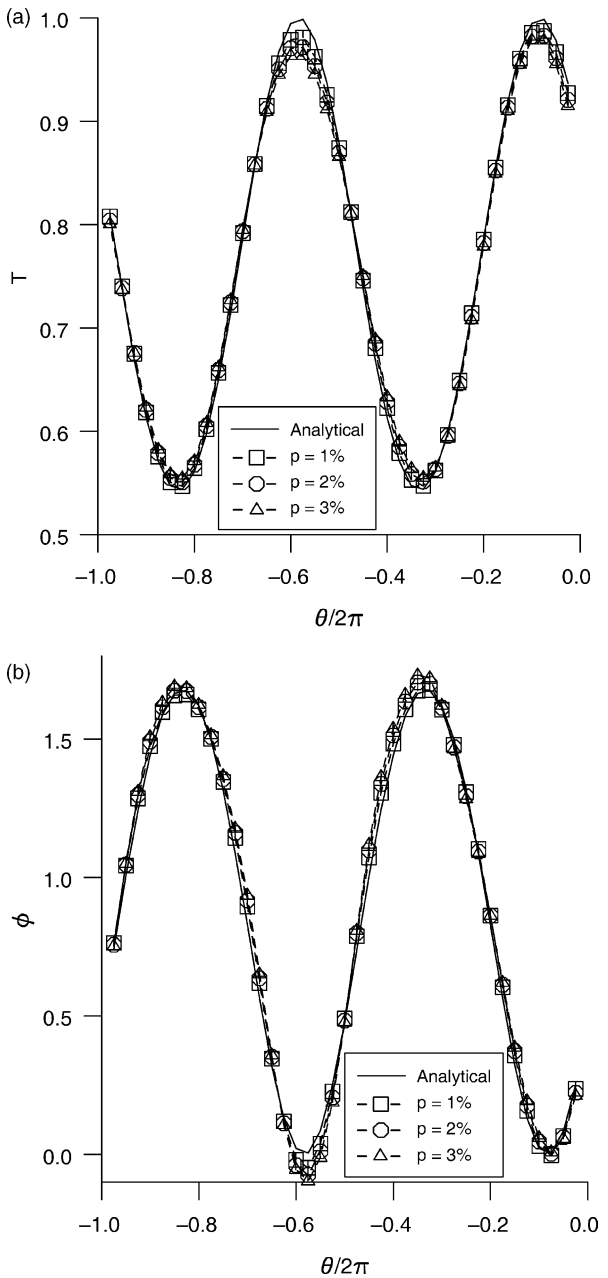

Fig. 7. (a) The analytical solution $T^{(an)}$ (—) and the numerical solution $T^{(num)}$, and (b) the analytical solution $\Phi^{(an)}$ (—) and the numerical solution $\Phi^{(num)}$, obtained with $N = 80$ boundary elements and various levels of noise $p = 1\%$ (–□–), $p = 2\%$ (–○–) and $p = 3\%$ (–△–) added into the input data $\tilde{T}|_{\Gamma_2}$, for Example 2.

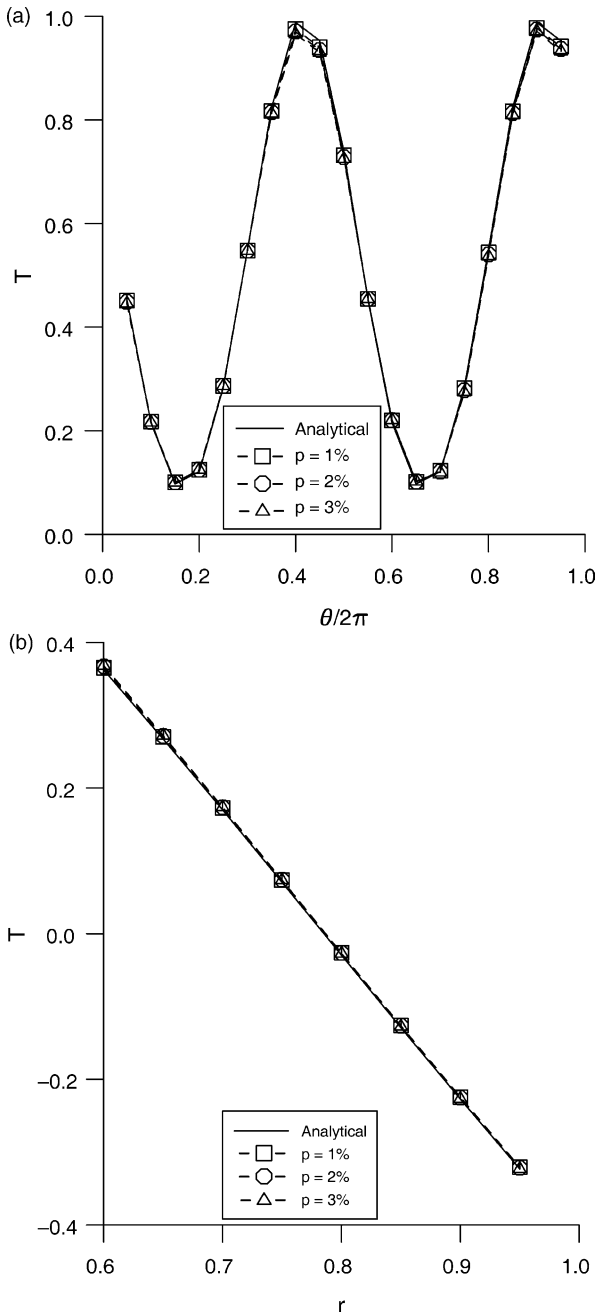

Fig. 8. The analytical solution $T^{(an)}$ (—) and the numerical solution $T^{(num)}$ obtained with $N = 80$ boundary elements and various levels of noise $p = 1\%$ (–□–), $p = 2\%$ (–○–) and $p = 3\%$ (–△–) added into the input data $\tilde{T}|_{\Gamma_2}$, at the internal points (a) $\underline{x} \in \Gamma_r$, and (b) $\underline{x} \in \Gamma_\theta$, for Example 2.

Table 1 which presents the errors e_T and e_Φ, as well as the optimal iteration number n_{opt} given by the stopping criterion described in Section 5.3 obtained with various levels of noise added into the input temperature data and various iterative regularization methods, namely the Landweber method studied in this paper, the alternating iterative method presented in Ref. [15] and the CGM described in Ref. [16], for both Examples 1 and 2. For Example 2, no results are presented for the alternating algorithm which is divergent since the operator $\mathscr{L} \equiv \Delta + \alpha^2$, $\alpha \in \mathbb{R}$, is not positive definite.

Table 1
The errors e_T and e_Φ and the value of the optimal iteration number n_{opt} obtained with $N = 80$ boundary elements, various amounts of noise added into the input data $T|_{\Gamma_2}$, namely $p \in \{0, 1, 2, \}$, and several iterative regularization methods, for Examples 1 and 2

Example	Method	Error	$p = 0\%$	$p = 1\%$	$p = 2\%$
Example 1	Landweber	e_T	1.38×10^{-1}	2.48×10^{-1}	3.55×10^{-1}
		e_Φ	6.78×10^{-1}	1.07×10^{0}	1.40×10^{0}
		n_{opt}	153	112	93
	Alternating algorithm	e_T	1.30×10^{-1}	2.30×10^{-1}	3.35×10^{-1}
		e_Φ	6.51×10^{-1}	1.01×10^{0}	1.31×10^{0}
		n_{opt}	14	10	8
	CGM	e_T	1.04×10^{-1}	2.24×10^{-1}	2.83×10^{-1}
		e_Φ	6.21×10^{-1}	9.75×10^{-1}	1.22×10^{0}
		n_{opt}	3	3	2
Example 2	Landweber	e_T	1.33×10^{-2}	2.09×10^{-2}	2.79×10^{-2}
		e_Φ	5.89×10^{-2}	8.41×10^{-2}	1.07×10^{-1}
		n_{opt}	286	238	209
	CGM	e_T	7.01×10^{-3}	1.38×10^{-2}	2.05×10^{-2}
		e_Φ	5.67×10^{-2}	8.13×10^{-2}	9.86×10^{-2}
		n_{opt}	3	2	2

From the numerical results presented in this section, it can be concluded that the stopping criterion developed in Section 5.3 has a regularizing effect and the numerical solution obtained by the iterative BEM described in this paper is convergent and stable with respect to refining the mesh size and decreasing the level of noise added into the input data, respectively, for both boundary and internal points.

6. Conclusions

In this paper, we have investigated the Cauchy problem for Helmholtz-type equations in the two-dimensional case. In order to deal with the instabilities of the solution of this ill-posed problem, an iterative Landweber BEM was employed which reduced the Cauchy problem to solving a sequence of well-posed boundary value problems in the space of square integrable functions, thus enabling the numerical representation. A stopping criterion, necessary for ceasing the iterations at the point where the accumulation of noise becomes dominant and the errors in predicting the exact solution increase, has also been presented. The numerical results obtained for various numbers of boundary elements and various amounts of noise added to the input data showed that the method produces a convergent, stable and consistent numerical solution with respect to increasing the number of boundary elements and decreasing the amount of noise.

The main advantage of the Landweber method is that it provides accurate, convergent and stable numerical solutions to the Cauchy problem associated with Helmholtz-type

equations, i.e. $\mathscr{L} \equiv \Delta + k^2$, in both cases, namely for $k \in \mathbb{R}$ and for $k \in \mathbb{C}\backslash\mathbb{R}$, unlike the alternating iterative method of Kozlov et al. [26] which fails to solve the Cauchy problem for the operator $\mathscr{L} \equiv \Delta + k^2$ for k real, see Ref. [15]. For our application, the disadvantages of the Landweber method consist of the relatively large numbers of iterations required to solve the problem in comparison with the other two regularization methods and the lower accuracy of the numerical solutions compared especially with the CGM, see Table 1. However, in other applications such as electrical capacitance tomography, see Ref. [27], the CGM does not give better results since it is less regularizing than the Landweber method, as demonstrated in Ref. [28]. Furthermore, the regularizing operators generated by the CGM are non-linear and, consequently, the proof of convergence for this method is more difficult and technical than that for the Landweber method, see Ref. [29].

Acknowledgements

L. Marin would like to acknowledge the financial support received from the EPSRC.

References

[1] Beskos DE. Boundary element method in dynamic analysis, Part II (1986–1996). ASME Appl Mech Rev 1997;50:149–97.
[2] Chen JT, Wong FC. Dual formulation of multiple reciprocity method for the acoustic mode of a cavity with a thin partition. J Sound Vib 1998;217:75–95.
[3] Harari I, Barbone PE, Slavutin M, Shalom R. Boundary infinite elements for the Helmholtz equation in exterior domains. Int J Numer Meth Eng 1998;41:1105–31.
[4] Hall WS, Mao XQ. A boundary element investigation of irregular frequencies in electromagnetic scattering. Eng Anal Bound Elem 1995;16:245–52.
[5] Kern DQ, Kraus AD. Extended surface heat transfer. New York: McGraw-Hill; 1972.
[6] Manzoor M, Ingham DB, Heggs PJ. The one-dimensional analysis of fin assembly heat transfer. ASME J Heat Transfer 1983;105:646–51.
[7] Wood AS, Tupholme GE, Bhatti MIH, Heggs PJ. Steady-state heat transfer through extended plane surfaces. Int Commun Heat Mass Transfer 1995;22:99–109.
[8] Chen G, Zhou J. Boundary element methods. London: Academic Press; 1992.
[9] Hadamard J. Lectures on Cauchy problem in linear partial differential equations. London: University Press; 1923.
[10] Bai MR. Application of BEM-based acoustic holography to radiation analysis of sound sources with arbitrarily shaped geometries. J Acoust Soc Am 1992;92:533–49.
[11] Kim BK, Ih JG. On the reconstruction of the vibro-acoustic field over the surface enclosing an interior space using the boundary element method. J Acoust Soc Am 1996;100:3003–16.
[12] Wang Z, Wu SR. Helmholtz equation-least-squares method for reconstructing the acoustic pressure field. J Acoust Soc Am 1997;102:2020–32.
[13] Wu SR, Yu J. Application of BEM-based acoustic holography to radiation analysis of sound sources with arbitrarily shaped geometries. J Acoust Soc Am 1998;104:2054–60.
[14] DeLillo T, Isakov V, Valdivia N, Wang L. The detection of the source of acoustical noise in two dimensions. SIAM J Appl Math 2001;61:2104–21.
[15] Marin L, Elliott L, Heggs PJ, Ingham DB, Lesnic D, Wen X. An alternating iterative algorithm for the Cauchy problem associated to the Helmholtz equation. Comput Meth Appl Mech Eng 2003;192:709–22.
[16] Marin L, Elliott L, Heggs PJ, Ingham DB, Lesnic D, Wen X. Conjugate gradient-boundary element solution to the Cauchy problem for Helmholtz-type equations. Comput Mech 2003;31:367–77.
[17] Landweber L. An iteration formula for Fredholm integral equations of the first kind. Am J Math 1951;73:615–24.
[18] Fridman VM. Method for successive approximation for a Fredholm integral equation of the first kind. Uspeki Math Nauka 1956;11:233–4. [in Russian].
[19] Engl HW, Hanke M, Neubauer A. Regularization of inverse problems. Boston: Kluwer; 1996.
[20] Craig EJ. The *N*-step iteration procedures. J Math Phys 1956;34:64–73.
[21] Shamanskii VE. On certain numerical schemes for iteration processes. Ukr Math Zh 1962;14:100–9. [in Russian].
[22] Nemirovskii AS. The regularizing properties of the adjoint gradient method in ill-posed problems. Comput Math Math Phys 1986;26:7–16.
[23] Johansson T. Reconstruction of a stationary flow from boundary data, Dissertation No. 853, Linköping, 2000.
[24] Wendland WL, Hsiao GC. On the integral equation for the plane mixed boundary value problem of the Laplacian. Math Meth Appl Sci 1979;1:265–321.
[25] Stephan EP. Boundary integral equations for mixed boundary value problems in $\mathbb{R}^3$. Math Nachr 1987;134:21–53.
[26] Kozlov VA, Maz'ya VG, Fomin AF. An iterative method for solving the Cauchy problem for elliptic equations. Comput Math Math Phys 1991;31:45–52.
[27] Liu S, Fu L, Yang WQ. Optimization of an iterative image reconstruction algorithm for electrical capacitance tomography. Meas Sci Technol 1999;10:L37–9.
[28] Yang WQ, Peng L. Image reconstruction algorithms for electrical capacitance tomography. Meas Sci Technol 2003;14:R1–R13.
[29] Hanke M. Conjugate gradient type methods for ill-posed problems. New York: Longman; 1995.